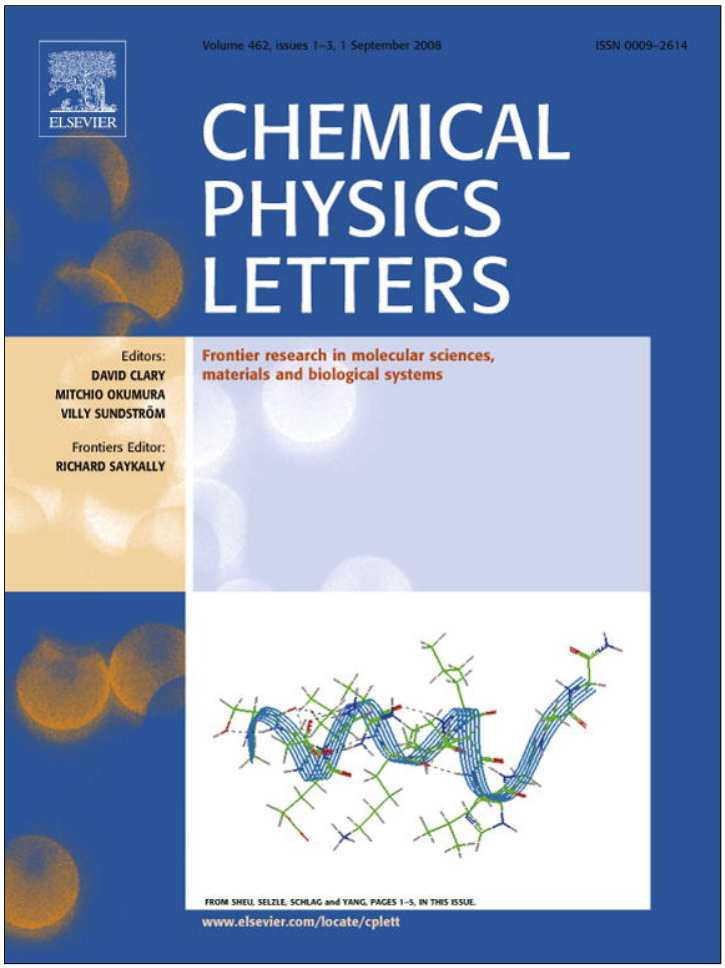

Chemical Physics Letters 462 (2008) 92–95

Contents lists available at ScienceDirect

Chemical Physics Letters

journal homepage: www.elsevier.com/locate/cplett

Oxygen-assisted shape control in polyol synthesis of silver nanocrystals

Atsushi Taguchi [a,*], Shintaro Fujii [b], Taro Ichimura [b,1], Prabhat Verma [c,1], Yasushi Inouye [c,1] Satoshi Kawata [a,b,1]

[a] Nanophotonics Laboratory, RIKEN, Wako, Saitama 351-0198, Japan
[b] Department of Applied Physics, Osaka University, Suita, Osaka 565-0871, Japan
[c] Department of Frontier Biosciences, Osaka University, Suita, Osaka 565-0871, Japan

ARTICLE INFO

Article history:
Received 17 May 2008
In final form 18 July 2008
Available online 29 July 2008

ABSTRACT

We have found that the shape of silver nanocrystals is conveniently controlled by injection of oxygen gas during the polyol reduction of silver ions. The presence of oxygen effectively promotes the oxidative etching of multiple twined particles. Adjusting the flow rate of the oxygen gas yields uniformly-sized silver nanocubes, right bipyramids, nanowires, and spherical nanoparticles depending on the injection rate of the oxygen gas. Electron diffraction and high resolution TEM observations of the synthesized nanocrystals show our nanocrystals do consist of silver, not of silver oxide. SERS activities of the synthesized nanocrystals were also examined.

1. Introduction

Metal nanoparticles play an important role in modern nanophotonics such as surface- and tip-enhanced Raman scattering (SERS and TERS) [1–7], enhancement and/or modification of single molecule fluorescence emission using an optical nanoantenna [8–14], and their applications to the nanoscale analysis and imaging [15–19]. The localized surface plasmon resonance supported by metal nanoparticles provides a strong and highly confined electromagnetic field, which is the primary principle behind the high sensitivity [20–22] and high resolution achieved by these techniques.

Recently, novel and interesting shapes of nanoparticle such as nanocubes, right bipyramids, and nanowires have been synthesized in a shape-controllable manner pioneered by Xia's group [23–25]. These shapes are not only fascinating but also attractive in applying them to construct SERS/TERS probes, nanoantennas, and associated plasmonic nanodevices. The uniform shape spontaneously determined by the crystalline facet can be an ideal building block to construct nanoscale structures with unprecedented accuracy and reliability which cannot be achieved by the techniques employed so far, such as vacuum deposition, lithography [7], and focused ion beam milling [9,26]. Also because the spectral properties of the plasmon resonance strongly depend on the shape of the metal nanoparticles [27–29], shape-selectivity in nanoparticle synthesis gives us an opportunity to fully explore the benefit of assembled plasmonic nanodevices in an efficient way for a given application.

Xia et al. employed polyol synthesis, in which metal ions are reduced by heated ethylene glycol (EG) with poly(vinyl pyrrolidone) (PVP) used primarily as a stabilizer to prevent aggregation of the colloidal particles as well as a function for regulating crystal growth [23,24]. They found corrosive salts such as HCl, NaCl and NaBr added into the reaction solution can work as an etching reagent against the deposited particles [25,30,31]. This oxidative etching preferentially removes thermodynamically (entropically) favorable multiple twined particles (MTP), and thermodynamically less favorable single crystalline nanocubes remain as the final product. Although factors such as the introduction of a capping agent can alter what is the thermodynamically most favorable structures, different types of crystalline structure essentially show different resistivities against oxidative etching. They tried different kinds of salts with different corrosiveness to adjust the etching power, and they could let the desired shape remain selectively, the others be etched out.

In this work, we report that the shape of polyol-synthesized nanoparticles can be controlled by direct injection of oxygen into the reaction solution. For the control of the etching efficiency, we simply adjusted the flow rate of the injected oxygen instead of changing etching reagents or adjusting concentrations of the reagents. We found that nanocubes, right bipyramids, nanowires, and spherical nanoparticles are selectively synthesized depending on the flow rate of oxygen. This result will contribute to simplification of the shape-controlled synthesis of metal nanoparticles. SERS activities and local field enhancement of the synthesized nanoparticles are also discussed.

* Corresponding author.
E-mail address: taguchi@riken.jp (A. Taguchi).
[1] Also at the CREST, Japan Corporation of Science and Technology (JST), Kawaguchi, Saitama 322-0012, Japan.

0009-2614/$ - see front matter © 2008 Elsevier B.V. All rights reserved.
doi:10.1016/j.cplett.2008.07.077

2. Experimental

2.1. Synthesis of metal nanoparticles

The synthetic procedure was as follows. 5 mL of EG (99.5+%, Wako) contained in a 30 mL beaker was heated up to 160 °C in a stirring oil bath for one hour to remove trace amounts of water before the reaction started. The reported Cl and Fe impurities contained in the EG were below 66 μM and 200 μM, respectively. Immediately after heating was started, an oxygen gas was started to pass through a glass pipet inserted into the EG with regulated flow rate. The flow rate was measured by a simple rotameter, typically set below 10 mL/min. The oxygen was bubbling up from the tip of the glass pipet immersed in the EG one by one with a moderate frequency and released into the air. After the pre-heating, 30 μL of EG solution containing 10 mM NaBr (99.9%, Wako) was added into the heated EG. Subsequently, two 3 mL EG solution, one containing 94 mM $AgNO_3$ (99.0+%, Aldrich) and the other containing 144 mM PVP (average Mw ≈ 55 000, Aldrich, concentration calculated in terms of the repeating unit) and 0.11 mM NaBr were simultaneously added by a two-channel syringe pump into the heated EG with the rate of 45 mL/h. During the reaction the beaker was capped with an aluminum cover having a small hole through which the pipet can be inserted. After two hours, the solution was taken out from the oil bath and naturally-cooled down to room temperature.

For recovering the nanoparticles, the solution was first diluted with acetone and centrifuged at 25 000 rpm for 10 min. The supernatant solution was substituted with clean acetone and sonicated for a minute, then the suspension was again centrifuged. This cleaning step was repeated several times with acetone, ethanol, and water. Finally the nanoparticles were recovered in water and used in the following experiments.

2.2. SERS and normal Raman measurements

4-Aminothiophenol (4-ATP) was used as a test molecule. Self assembled monolayer (SAM) of 4-ATP was formed on the synthesized silver nanocubes by the protocol described in literature [32]. Briefly, the suspension of silver nanocubes was dropped on a clean glass substrate and dried. The substrate was then immersed in 0.1 mM 4-ATP solution for four hours, then rinsed with ethanol to remove excess 4-ATP.

A Nd:YVO_4 laser with the wavelength of 532 nm was used for Raman excitations. The excitation laser was focused on the substrate surface with an objective with NA 1.4. The excitation power was typically 0.2 mW at the sample and the exposure time was set to 60 s. 2 μm × 2 μm area around the focus spot was scanned by atomic force microscope (AFM) to confirm that only one isolated single nanocube lies in the focus spot.

We also measured normal Raman spectra of solid 4-ATP. The same 4-ATP solution was dropped on a clean glass substrate and dried to form small solid 4-ATP islands. In this case, the excitation power was 4.6 mW at the sample. The exposure time was 120 s.

3. Results and discussion

3.1. Synthesis of silver nanocubes with oxygen

First, we injected the oxygen with a rate of 8 mL/min into the reaction solution. Immediately after the injection of silver precursor, the color of solution turned light yellow, which indicates the formation of silver nanoparticles. Four minutes after the reaction began, the color of the solution suddenly turned into transparent and colorless. This continued for approximately one minute. This phenomenon implies the silver nanoparticles were oxidatively etched and re-dissolved into the solution [30]. After five minutes, the color again began to turn yellow. The color gradually became strong in intensity. After 15 min, the solution became dark yellow and non-transparent. After 30 min, the solution became ocher in color, and this color was kept until the end of the reaction.

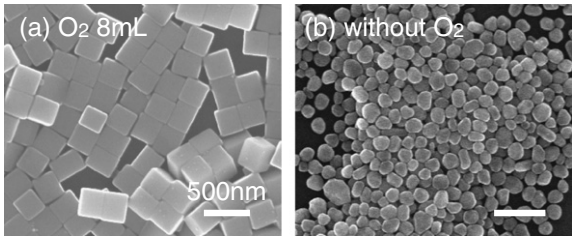

Fig. 1. SEM images of silver nanocubes that were synthesized (a) with 8 mL/min oxygen flow and (b) without oxygen flow. Scale bar is 500 nm.

The SEM image of the final product is shown in Fig. 1a. Almost all particles are single crystalline nanocubes. The average edge length is approximately 200 nm. We could not find any other types of twined particles.

Fig. 1b shows the final product obtained by the same reaction condition as Fig. 1a but without the oxygen injection. We see the main product was spherical MTPs. In this case, the color of the reaction solution became monotonically strong in its intensity, never became colorless as did in the case with oxygen flow. After 30 min the color became opaque milky yellow and this color remained until the end of the reaction (1 h 30 m). The fact that the color became opaque more quickly than the case of with oxygen indicates the presence of oxygen effectively promotes the oxidative etching and reduces the growing speed of nanoparticles.

3.2. Shape control by changing oxygen flow rate

When we varied the oxygen flow rate from 8 mL/min to 2 mL/min, drastic changes were observed in the crystalline shape of the final products. The results are shown in Fig. 2. In contrast with the case of 8 mL/min oxygen flow rate which gave almost 100% nanocubes (Fig. 1a), in the case of 6 mL/min, the main product was right bipyramids with occupancy of 60% (Fig. 2a). In the case of 4 and 2 mL/min flow rates, the main products were nanowires (80%) and spherical nanoparticles (90%), respectively (Fig. 2b and c).

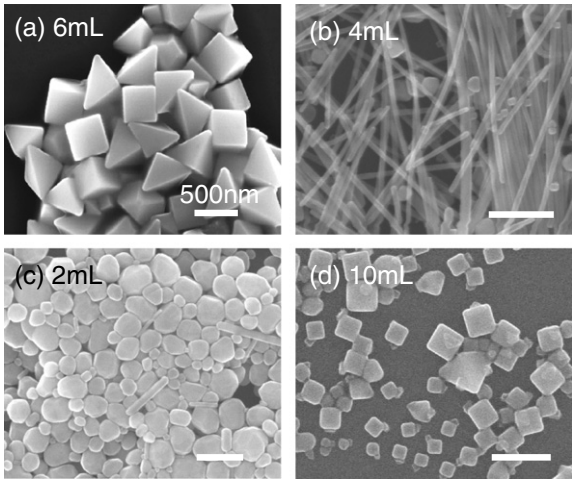

Fig. 2. SEM images of silver nanocrystals that were synthesized with the oxygen flow of 6 mL/min, (b) 4 mL/min, (c) 2 mL/min and (d) 10 mL/min. Scale bar is 500 nm.

A clear correlation was found between the injection rate of the oxygen and the amount of the twin defects in the crystalline structure of the final product. Crystallographic studies have revealed that nanocubes are grown from single crystalline seeds with no twin defect, right bipyramids are from single twined seeds, nanowires are from decahedral twined seeds, and spherical particles are from multiple twined seeds with many twin defects, respectively [24,28]. Because the defects provide active sites for oxidative dissolution, more defect-rich particles are more active and corrosion-prone for oxidative etching [30,33]. Thus, spherical MTPs are considered to be the most easily etched, nanowires come next, right bipyramids, and nanocubes are the most resistive to oxidative etching. On the other hand, more defect-rich particles are thermodynamically more favorable under natural conditions without the influence of oxidative etching. These two opposing trends are balanced in the presence of oxygen, which results in the shape selectivity observed here.

In the current experimental system, because a large portion of the injected oxygen was released into the air, it is difficult to precisely relate the efficiency of undergoing oxidative etching to the actual concentration of the oxygen dissolved in the EG. As a rough measure, we evaluated that the oxygen of 4 mL/min is sufficient to etch out the multiple twined seeds but not sufficient to eliminate the decahedral twined seeds (Fig. 2b). Similarly, 6 mL/min oxygen etches out decahedral twined particles but does not for single twined particles (Fig. 2a). 8 mL/min oxygen etches out all twined particles (Fig. 1a). We are now working with the improvement of the system to enable direct evaluation of the oxygen concentration in EG.

Too much oxygen gave undesirable influence on the uniformity of the final product. When we tried the oxygen flow rate of over 10 mL/min, the final product was again dominated by nanocubes, however, the size of the cubes were widely distributed ranging from 80 nm to 200 nm (Fig. 2d). This implies that the nanocubes were partly etched owing to the exceedingly increased etching efficiency.

The successful production of nanowires in the presence of oxygen in the case of 4 mL/min oxygen flow is noticeable because Xia and co-workers publishes some reports stating that oxygen must be removed or scavenged from the system in order for the decahedral twined seeds to stay around long enough to grow into nanowires [34,35]. We attributed the production of nanowires to the large amount of Fe as much as 200 μM contained in the EG used in our synthesis. As Xia et al. pointed out, Fe(II) can remove atomic oxygen adsorbed on the surface of the silver, thus can work as a blocking agent gainst the oxidative etching. As the result, in our reaction condition, the oxidative etching was rather suppressed to a considerably low level when the oxygen flow rate was set at low. This suppressed state helped the decahedral twined seeds to grow into nanowires. The inhibited oxidative etching was then reactivated with increasing the oxygen flow rate, providing the means to control oxidative etching efficiency depending on the flow rate of the oxygen injection and the shape selectivities emerged.

If the competition between the adsorbed oxygen etching silver atoms and its inhibitor Fe(II) is a key mechanism for the observed variation of the oxidative etching efficiency, varying oxygen flow rate should result in a variation in oxidative etching rate, rather than etching power. Indeed, a relation between the oxygen flow rate and the etching rate becomes apparent when comparing the timing at which the color of the reaction solution turned colorless. In the case of 8 ml/min, the color completely vanished at around three minutes and a half. In contrast, in the case of 6 and 4 mL/min, the light yellow turned colorless at around four minutes and a half, slower than the case of 8 mL/min. For 2 mL/min case, the yellow color slightly faded at around four minutes and a half but never turned colorless. For the case of no oxygen injection, the color kept monotonically increasing in its intensity, which indicates no oxidative etching occurred. Because only the crystal seeds that are growing faster than the rate of undergoing oxidative etching remain as a final product, increasing/decreasing the rate of etching doesn't just result in taking a shorter/longer time for the twinned seeds to be removed.

The presence of Fe(III) can be another possible etching reagent against silver. However, this etching route had only a limited effect because silver and Fe(III) have values of the redox potential very close each other, and direct exchange of electron between these two was not likely to be involved. Also, the concentration of Fe(III) was limited by the amount of residual Fe, which is further reduced by the reduction process of Fe(III) to Fe(II) by EG, thus the generation rate of Fe(III) is not likely to be sufficient to become a main driving force of the etching.

During the preparation of this Letter, Xia and co-workers reported a new finding on the role of oxygen in the polyol synthesis of silver nanostructures, in which it was claimed that increasing the oxygen concentration in the polyol synthesis results in the increased amount of glycolaldehyde (GA) present in the reaction solution, where GA may serve as a reductant of metal ions [36]. The increased amount of GA should accelerate the growing speed of nanoparticles. In our case, however, the oxygen injection reduced the varying speed of the solution color during the reaction. This indicates that the growing speed of silver crystals was reduced by the oxidative etching effect rather than accelerated by the increased GA. Thus, the oxidative etching dominantly governed the reaction, and the effect of increased GA is considered to be limited in our synthesis. This difference was caused by the different concentration of oxygen in the reaction solution. In our case, the oxygen was injected with a moderate flow rate, while Xia *et al.* showed an evidence of increased GA at the saturated concentration of oxygen.

Finally, the role of Br^- in the synthesis has not yet been revealed clearly and now under investigation. Without adding NaBr, the syntheses were typically ended with the mixture of nanowires and MTPs, which suggests Br^- play some nonnegligible roles in the reaction.

3.3. TEM characterizations and SERS measurements of synthesized nanoparticles

In order to assess whether our nanoparticles truly consist of silver or silver oxide, we performed TEM analysis of the synthesized nanoparticles. Fig. 3a shows the high resolution TEM image of the nanocube obtained by 8 mL/min oxygen flow. We see the nanocube is composed of a single crystal with well-resolved lattice fringe spacing. The fringe spacing is 2.4 Å, corresponding to the lattice distance of {111} surfaces of silver. Fig. 3b shows a typical electron diffraction pattern taken from an individual nanocube.

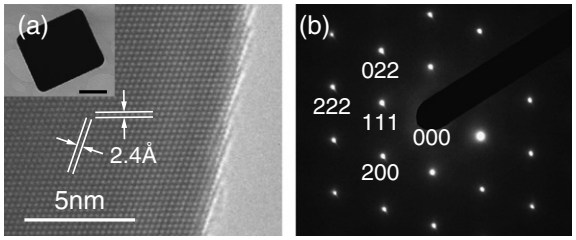

Fig. 3. (a) HRTEM image and (b) electron diffraction pattern of silver nanocube synthesized with oxygen. Inset in (a) shows a low magnification TEM image of the nanocube. Scale bar is 100 nm.

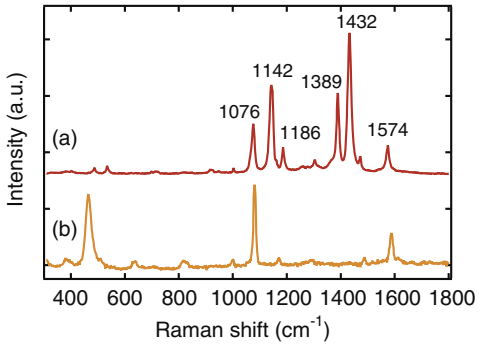

Fig. 4. (a) SERS spectrum of 4-ATP monolayer adsorbed on the silver nanocube synthesized with oxygen flow. (b) Normal Raman spectrum of solid 4-ATP.

The electron beam was directed along $Z = [011]$. The electron diffraction pattern clearly shows the fcc structure of silver. These results are direct evidences showing the synthesized nanocube consists of silver and not the silver oxide.

Finally, we examined SERS activities of our nanocubes by measuring SERS of 4-ATP SAM formed on the surface of nanocubes. The measured SERS spectrum is shown in Fig. 4a. The agreement of the peak frequencies and their relative intensities are excellent with the reported SERS spectra of the same 4-ATP monolayer formed on silver particles [32]. All SERS peaks can be assigned to the vibrational modes of 4-ATP. We compared the SERS spectrum with a normal Raman spectrum of solid 4-ATP deposited on a glass substrate, which is shown in Fig. 4b. The enhancement of four peaks at 1142, 1389, 1432, 1574 cm^{-1} originates from the metal-molecule charge transfer (CT) mechanism [32,37,38]. If the surface of the nanocubes is oxidized, the CT enhancement should be quenched [38]. The observation of the CT enhancement suggests again that the surface of our nanocubes is unlikely to be oxidized.

The enhancement of the 1076 cm^{-1} peak observed in the SERS spectrum is considered to be purely electromagnetic-origin and insensitive to the CT effects [32,37]. The comparison of this vibrational mode between SERS and normal Raman spectra provides an estimation of the electromagnetic field enhancement factor of the nanocubes. We assumed 4-ATP SAM covers the whole surface of a 200 nm nanocube, and its number density is $\sim 5\ nm^{-2}$ [32]. For the normal Raman case, we first estimated the number of the detected molecules from the volume of the solid 4-ATP in the excitation laser focus which was directly measured by an AFM. The density of solid 4-ATP of 1.18 g/cm^3 was used. The Raman enhancement factor was estimated to be 2.0×10^4, which resulted in the electromagnetic field enhancement of factor 14, where $|E|^4$ rule was adopted. These values are on a whole-surface average. The Raman enhancement at the local hot site provided by the sharp corner of nanocubes can be several orders of magnitude higher than the averaged value [27,29], which has more essential importance in applications to tip-enhancement.

4. Conclusion

We have shown that the shape of silver nanocrystals can be conveniently controlled by injection of oxygen gas during the polyol reduction of silver ions. By adjusting the oxidative etching rate, which can be adjusted by the flow rate of the oxygen, nanocubes, right bipyramids, nanowires, and spherical nanoparticles can be selectively obtained. Our nanoparticles are SERS active and no evidence was found that infers the silver is oxidized. We believe that this finding will greatly simplify the shape-controlled synthesis of silver nanoparticles in laboratories as well as in industrial mass production settings.

Acknowledgement

A part of the present experiments was carried out by using a facility in the Research Center for Ultrahigh Voltage Electron Microscopy, Osaka University.

This work was supported in part by a grant from the Japan Science and Technology Agency under a CREST (Core Research for Evolutional Science and Technology) project 'Plasmonic Scanning Analytical Microscopy'.

References

[1] S. Kawata (Ed.), Near-Field Optics and Surface Plasmon Polaritons, Springer, 2001.
[2] Y. Inouye, S. Kawata, Opt. Lett. 19 (1994) 159.
[3] N. Hayazawa, Y. Inouye, Z. Sekkat, S. Kawata, Opt. Commun. 183 (2000) 333.
[4] N. Hayazawa, T. Yano, H. Watanabe, Y. Inouye, S. Kawata, Chem. Phys. Lett. 376 (2003) 174.
[5] R.M. Stöckle, Y.D. Suh, V. Deckert, R. Zenobi, Chem. Phys. Lett. 318 (2000) 131.
[6] M. Moskovits, Rev. Mod. Phys. 57 (1985) 783.
[7] J.A. Dieringer et al., Faraday Discuss. 132 (2006) 9.
[8] T. Kalkbrenner, M. Ramstein, J. Mlynek, V. Sandoghdar, J. Microsc. 202 (2001) 72.
[9] J.N. Farahani, D.W. Pohl, H.J. Eisler, B. Hecht, Phys. Rev. Lett. 95 (2005) 017402.
[10] S. Kühn, U. Håkanson, L. Rogobete, V. Sandoghdar, Phys. Rev. Lett. 97 (2006) 017402.
[11] P. Anger, P. Bharadwaj, L. Novotny, Phys. Rev. Lett. 96 (2006) 113002.
[12] T.H. Taminiau, R.J. Moerland, F.B. Segerink, L. Kuipers, N.F. van Hulst, Nano Lett. 7 (2007) 28.
[13] T.H. Taminiau, F.D. Stefani, F.B. Segerink, N.F. van Hulst, Nat. Photonics 2 (2008) 234.
[14] R.J. Moerland, T.H. Taminiau, L. Novotny, N.F. van Hulst, L. Kuipers, Nano Lett. 8 (2008) 606.
[15] A. Hartschuh, E.J. Sánchez, X.S. Xie, L. Novotny, Phys. Rev. Lett. 90 (2003) 095503.
[16] T. Ichimura, N. Hayazawa, M. Hashimoto, Y. Inouye, S. Kawata, Phys. Rev. Lett. 92 (2004) 220801.
[17] N. Anderson, A. Hartschuh, S. Cronin, L. Novotny, J. Am. Chem. Soc. 127 (2005) 2533.
[18] T. Yano, P. Verma, S. Kawata, Y. Inouye, Appl. Phys. Lett. 88 (2006) 093125.
[19] C. Höppener, L. Novotny, Nano Lett. 8 (2008) 642.
[20] S. Nie, S.R. Emory, Science 275 (1997) 1102.
[21] K. Kneipp, Y. Wang, H. Kneipp, L.T. Perelman, I. Itzkan, R.R. Dasari, M.S. Feld, Phys. Rev. Lett. 78 (1997) 1667.
[22] T. Ichimura, H. Watanabe, Y. Morita, P. Verma, S. Kawata, Y. Inouye, J. Phys. Chem. 11 (2007) 9460.
[23] Y. Sun, Y. Xia, Science 298 (2002) 2176.
[24] B. Wiley, Y. Sun, B. Mayers, Y. Xia, Chem. A Eur. J. 11 (2005) 454.
[25] B.J. Wiley, Y. Xiong, Z.Y. Li, Y. Yin, Y. Xia, Nano Lett. 6 (2006) 765.
[26] P. Mühlschlegel, H.J. Eisler, O.J. Martin, B. Hecht, D.W. Pohl, Science 308 (2005) 1607.
[27] K.L. Kelly, E. Coronado, L.L. Zhao, G.C. Schatz, J. Phys. Chem. B 107 (2003) 668.
[28] B.J. Wiley, S.H. Im, Z.Y. Li, J. McLellan, A. Siekkinen, Y. Xia, J. Phys. Chem. B 110 (2006) 15666.
[29] J.M. McLellan, A. Siekkinen, J. Chen, Y. Xia, Chem. Phys. Lett. 427 (2006) 122.
[30] B. Wiley, T. Herricks, Y. Sun, Y. Xia, Nano Lett. 4 (2004) 1733.
[31] S.H. Im, Y.T. Lee, B. Wiley, Y. Xia, Angew. Chem. Int. Ed. 44 (2005) 2154.
[32] Y. Wang, H. Chen, S. Dong, E. Wang, J. Chem. Phys. 124 (2006) 74709.
[33] F.B. de Mongeot, A. Cupolillo, U. Valbusa, M. Rocca, Chem. Phys. Lett. 270 (1997) 345.
[34] B. Wiley, Y. Sun, Y. Xia, Langmuir 21 (2005) 8077.
[35] K.E. Korte, S.E. Skrabalak, Y. Xia, J. Mater. Chem. 18 (2008) 437.
[36] S.E. Skrabalak, B.J. Wiley, M. Kim, E.V. Formo, Y. Xia, Nano Lett. 8 (2008) 2077.
[37] M. Osawa, N. Matsuda, K. Yoshii, I. Uchida, J. Phys. Chem. 98 (1994) 12702.
[38] A. Otto, I. Mrozek, H. Grabhorn, W. Akemann, J. Phys. Condens. Matter 4 (1992) 1143.